CANADIAN JOURNAL OF REMOTE SENSING
2017, VOL. 43, NO. 2, 124–139
http://dx.doi.org/10.1080/07038992.2017.1286937

Taylor & Francis
Taylor & Francis Group

Modeling 3D Canopy Structure and Transmitted PAR Using Terrestrial LiDAR

Renato Cifuentes[a], Dimitry Van der Zande[b], Christian Salas[c], Laurent Tits[d], Jamshid Farifteh[e], and Pol Coppin[a]

[a]Department of Biosystems, KU Leuven, Division of Crop Biotechnics, Willem de Croylaan 34, Leuven BE-3001, Belgium; [b]Royal Belgian Institute of Natural Sciences, Directorate Natural Environment, Gulledelle 100, Brussels BE-1200, Belgium; [c]Departamento de Ciencias Forestales, Laboratorio de Biometría, Universidad de La Frontera, P.O. Box 54-D, Temuco, Chile; [d]Flemish Institute for Technological Research (VITO), Remote Sensing Unit, Boeretang 200, Mol BE-2400, Belgium; [e]Department of Geoinformation Processing, Faculty of Geo-Information Science and Earth Observation (ITC), University of Twente, P.O. Box 217, Enschede 7500 AE, The Netherlands

ABSTRACT

The heterogeneity and 3-dimensional (3D) organization of forest canopy elements is highly linked with the spatial variability of within and below canopy light. Using terrestrial LiDAR we studied the influence of several parameters in efficiently building 3D canopy models, and quantified below canopy light in 2 forest stands using ray-tracing. A voxel-based approach was used for canopy modeling, and a series of forest scenes were built for calculation of simulated structural variables (e.g., leaf area index, canopy openness). Through hypothesis testing, we found that simulated variables were consistent with the observed ones depending on: forest type, voxel size utilized in 3D modeling, and the zenith angle ranges used for calculations. Following below canopy light simulations were performed considering these 3 aspects. On average, estimates of light being transmitted overestimated measured light, and variance in below canopy light was maximum at lower values of measured light. This study presented a method to objectively define 3D modeling parameters for an efficient characterization of canopy structure, allowing to simulate trends in radiation flux transmitted to the forest floor. Improvements in the modeling process and ray-tracing parameterization were suggested.

RÉSUMÉ

L'hétérogénéité et l'organisation tridimensionnelle (3D) des éléments du couvert forestier sont fortement liées à la variabilité spatiale de la lumière à l'intérieur et sous le couvert forestier. En utilisant le LiDAR terrestre, nous avons étudié l'influence de plusieurs paramètres pour construire efficacement des modèles 3D du couvert forestier, et nous avons quantifié la lumière sous le couvert forestier dans deux peuplements de forêts en utilisant une méthode de ray-tracing. La modélisation par voxel a été utilisée pour représenter le couvert forestier et une série de scènes forestières a été construite pour le calcul de variables structurales simulées (par exemple, l'indice de surface foliaire, l'ouverture du couvert). Grâce à des tests d'hypothèses, nous avons constaté que les variables simulées étaient cohérentes avec celles observées en fonction du type de forêt, de la taille du voxel utilisée dans la modélisation 3D et des plages d'angles zénithaux utilisées pour les calculs. Les simulations de la lumière sous le couvert forestier ont été réalisées en tenant compte de ces trois aspects. En moyenne, les estimations de la lumière transmise présentaient une surestimation de la lumière mesurée et la variance de la lumière sous le couvert forestier était maximale à des valeurs inférieures de la lumière mesurée. Cette étude a présenté une méthode permettant de définir objectivement les paramètres de modélisation 3D pour une caractérisation efficace de la structure du couvert, permettant de simuler les tendances du flux de rayonnement transmis au sol de la forêt. Des améliorations ont été suggérées pour le processus de modélisation et pour la paramétrisation de la méthode du ray-tracing.

ARTICLE HISTORY
Received 30 August 2016
Accepted 14 December 2016

Introduction

Forest canopy is a unique part of forest ecosystems where fundamental interactions between vegetation and the physical environment take place. These interactions drive forest productivity, which is closely linked to biodiversity richness (Waide et al. 1999) and can be used to explain how forest health and dynamics are affected by, for example, climate change. The structure of forest canopies influences solar radiation interception and transmittance, depending on the amount of incident solar radiation at a particular incident angle, the spectral properties of tree elements, and the location and dimension of canopy gaps (Holbrook and Lund 1995). Therefore, behavior of key variables in estimating forest productivity are connected with the heterogeneity and 3-dimensional (3D) structure of canopies (Gobron and Verstraete 2009). A key variable is the fraction of photosynthetically active radiation (PAR) in the 400 nm–700 nm spectral range that a plant canopy absorbs for photosynthesis and growth. The

CONTACT Renato Cifuentes renato.cifuentes@kuleuven.be

impact of canopy structure on solar radiation interception and transmittance can be quantified using 3D radiative transfer models (Cescatti 1997). Part of the required inputs for developing such models encompass accurate descriptions of canopy structure, crown shapes, leaf density, and spatial distribution of leaf area (Law et al. 2001). Difficulties in accessing forest canopy, however, impose severe limitations for direct sampling and quantification of its structure and, therefore, an accurate representation of its spatial variation is hard to achieve (Parker 1995).

Ground-based light detection and ranging (LiDAR) systems provide an effective approach to characterize forest canopies in 3D (Dassot et al. 2011; Hilker et al. 2010; Hopkinson et al. 2004; Moskal and Zheng 2012; Strahler et al. 2008; Zhao et al. 2012). This is achieved using a detailed 3D representation of the forest structure generated through a non-destructive, objective, and reproducible manner (Cifuentes et al. 2014a; Hosoi and Omasa 2007; Jupp et al. 2009; Moorthy et al. 2008; Seidel et al. 2012; Van Leeuwen et al. 2011). Individual trees have been reconstructed using terrestrial laser scanning (TLS) data (Côté et al. 2009; Raumonen et al. 2013), or from TLS data combined with tree modeling software to delineate individual crowns (Da Silva et al. 2012; Van der Zande et al. 2011; Van Leeuwen et al. 2013). A limited number of studies, however, have utilized 3D canopy structural data to model and study radiation interactions within clumped broadleaved forest canopies. Bittner et al. (2012) used a TLS-based voxel representation of an experimental juvenile beech stand to simulate the light environment. Similarly, 3D representations of oak stands were generated and within-canopy light interception was modeled through time in Van der Zande et al. (2010). Results of this study highlighted the potential of a voxel-based representation of forest canopies derived from LiDAR measurements to study radiation interactions. In order to build suitable 3D models from TLS-derived data, an optimized processing procedure is introduced aiming at: (*i*) address the influence that noise has on the quality of these data sets (Maas et al. 2008), (*ii*) perform an accurate point cloud classification (Pfeifer et al. 2004), and (*iii*) define an efficient representation of the tree geometries (Dassot et al. 2012). First, noise due to range ambiguity, i.e., when the laser beam is illuminating partially 2 surfaces with different distances from the sensor (Massaro et al. 2014), is commonly minimized by removing the erroneous points (also known as ghost points) based on the range difference with respect to neighboring points (Cifuentes et al. 2014b). Phase-based scanning delivers extra noise originated at clear beam paths (e.g., open sky or canopy gaps), where instead of registering a no-hit, random range measurements are recorded (Newnham et al. 2012). Secondly, TLS using monochromatic laser light are limited in terms of point classification possibly affecting the quality of the derived canopy 3D models. Point cloud classification between foliage and woody material is straightforward when using, for example, TLS with full-waveform of back scattered energy at 2 wavelengths in the near (1,063 nm) and middle infrared (1,545 nm) parts of the electromagnetic spectrum (Danson et al. 2014; Yang et al. 2013), or at 1,500 nm (Côté et al. 2011). Other TLS, however, may depend on more complex point cloud classification methods, such as covariance matrix analysis (Belton and Lichti 2006), object-based (Zhang and Lin 2012), or dimensionality analysis (Demantké et al. 2009). Partitioning methods using octree-based algorithms (Jackins and Tanimoto 1980; Szeliski 1993) have also been used as a way of segmenting LiDAR point clouds (Wang and Tseng 2004, 2011) and was implemented on the processing chain. Finally, to limit data dimensionality and obtain a proper representation of the tree geometries, leaves or clump of leaves were represented as planar polygons (e.g., triangles, discs or ellipses; Huang et al. 2013; Stuckens et al. 2009a).

The main advantage of 3D simulation models is that the effect of a number of variables can be studied independently across a wide range of parameter values and canopy scenarios (Disney et al. 2010). For instance, feeding canopy models with reliable information about foliage light interception would allow, for example, simulation of photosynthetic carbon uptake and net ecosystem gas exchange (i.e., transpiration and evaporation) in response to climatic and nutritional conditions (Ågren et al. 1991; Medlyn et al. 2003; Mercado et al. 2007). Similarly, an accurate characterization of the radiation regime within the forest canopy can be used as input to energy-balance models (Hardy et al. 2004).

The reliability of 3D models representing canopy structure were assessed by comparing observed and simulated structural variables, such as effective leaf area index (LAI), clumping index (Ω), and canopy openness (CO). These variables can be estimated using hemispherical photography and are broadly used to characterize forest canopy structure and assess understory illumination (Gonsamo et al. 2010; Jennings et al. 1999; Walter et al. 2003; Weiss et al. 2004), providing useful information to understand canopy-radiation interactions (Korhonen et al. 2011; Parker 1995). Hemispherical photographs were taken and used as a validation tool for the LiDAR-based retrievals after 3D modeling. Consequently, and besides the traditional use of the coefficient of determination (R^2), hypothesis testing was conducted in the present study to determine whether there was a significant linear relationship between observed structural variables obtained from

reference hemispherical photography and simulated structural variables retrieved from the TLS-based 3D models. This work aimed to: (*i*) develop a methodology to build a set of 3D models that efficiently represented LAI, Ω, and CO of 2 different forest stands, and (*ii*) select and use one of the models that were built for each forest stand to perform canopy-light interaction analysis establishing observed versus simulated transmitted PAR (PAR_t) relationships.

Materials and methods

Study site

The field measurements were conducted in the Heverlee Forest (Heverlee-Meerdaal complex). The complex covers a total area of approximately 1,890 ha and is the second largest forest complex in Flanders, Belgium (50° 51′ N, 4° 40′ E, 60 m above mean sea level). Data were collected on a pure beech (*Fagus sylvatica* L.) forest stand and on a mixed forest stand (Figure 1), formed mainly by a combination of 3 species: beech, oak (*Quercus robur* L.), and birch (*Betula pendula* Roth). Both pure beech and mixed forests are located in a generally flat terrain where no understory was present. The average stand variables represent typical forest conditions in the study areas and were estimated based on 3 sample plots of 250 m^2 in the mixed forest (3.0 ha), and 3 sample plots of 500 m^2 in the beech forest (2.5 ha). Different plot sizes were used given the tree density and diameter at breast height in each forest stand, while the number of plots was selected due to their homogeneity, and considering a minimum sampling intensity of 3%. Respectively, mixed and beech forests have a density of 675 stems ha^{-1} and 223 stems ha^{-1}, a basal area of 21.0 m^2 ha^{-1} and 28.6 m^2 ha^{-1}, a quadratic mean diameter of 19.9 cm and 40.4 cm, a mean height of 23.1 m and 32.3 m, and a height to crown base of 7.1 m and 14.3 m.

Digital hemispherical photography

Digital hemispherical photographs (HP) of the canopy were acquired for each forest with a 6.1 MP Kodak DCS 660 digital camera, with a 180° fisheye lens (8 mm, f/4). The camera and lens were placed on a tripod 1.3 m above the ground and leveled using a double axis spirit level. The camera was oriented towards zenith with the magnetic north always located at the top of the image (Jonckheere et al. 2004). HPs were taken within a 30-minute period in each forest and before sunset (i.e., before 21h00) on a systematic geometrical pattern as suggested by Cifuentes et al. (2014a). A total of 9 positions per forest were used to take HPs on a 10-m grid within a 20 m × 20 m plot. These data were collected under overcast sky conditions to ensure homogeneous illumination of the canopy (Easter and Spies 1994; Gendron et al. 2006) on June 2014 (day of year) DOY173.

Below-canopy sampling of global irradiance

A remote cosine-corrected receptor (RCR) foreoptic attached to a FieldSpec® 3 spectroradiometer was used to measure instantaneous global irradiance (W m^{-2}) below forest canopy. The instrument measures the incoming radiation from 350 nm to 2,500 nm with a spectral resolution of 3 nm in the 350 nm–1,050 nm range and 10 nm in the 1,050 nm–2,500 nm range. In the present study, only solar radiation within the 400 nm–700 nm range (i.e., PAR_t) was used for further analysis. The RCR foreoptic was placed on a telescopic pole and leveled at 2.1-m height to avoid operator's partial blocking of the illumination, including diffuse skylight or light scattered

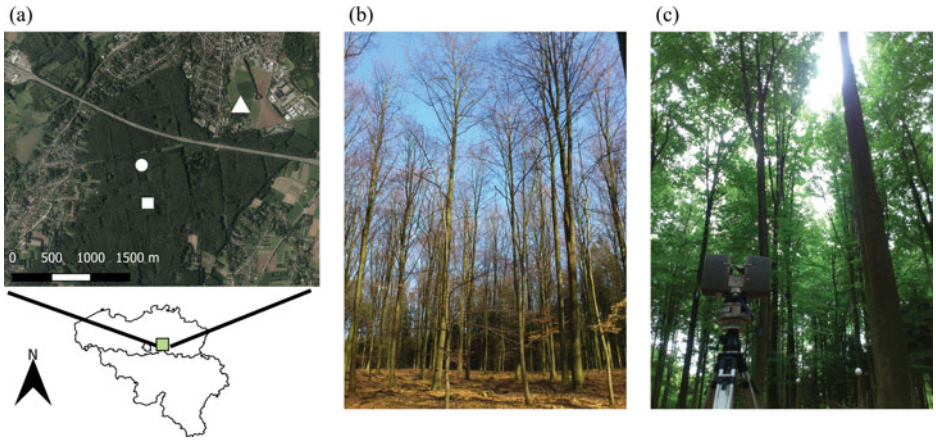

Figure 1. Location of study area. (a) Heverlee forest where beech (white square), mixed forests (white circle), and reference measurements of irradiance (white triangle) were located (source orthophoto: Informatie Vlaanderen); (b) leaf-off image of the mixed forest; and (c) leaf-on image of the beech forest and TLS instrument.

from surrounding objects. The base of the RCR has built-in bubble levels for its horizontal alignment.

The measurements were taken on every cross point of a 1-m grid on the 20 m × 20 m plot beneath each forest. At each measuring position (441 per forest) and for averaging purposes, 3 measurements were taken within a 5-second time frame, thus minimizing noise variability resulting from measuring below forest canopies (Giuliani and Brown 2008). The total amount of incoming radiation was measured simultaneously and continuously in the nearest open area, 1.7 km North-East from the study site (Figure 1a), using an HR-1024 spectroradiometer. These data were used to monitor anomalies in solar radiation due to clouds or aerosols, and to derive incoming PAR (PAR_i). Data were collected on June 2014, DOY163 and DOY164, within a 2-hour period around local solar noon, corresponding to a sun elevation angle range between 60° and 62°. Sky conditions were mostly clear, i.e., not opaque clouds, but occasional presence of transparent clouds on both dates. Average wind speed of 0.94 m/s and 1.1 m/s with predominant wind direction W and S-SW, on DOY163 and DOY164, respectively. Sunlight was blocked at the moment irradiance data were recorded during time periods when sky hemisphere was partly covered by clouds. For further analysis, a percentage of these noisy data were removed, retaining 67.4% (n = 297) and 80.1% (n = 353) of the total number of global irradiance measurements in mixed and beech forest, respectively.

TLS measurements and processing

TLS measurements were done on a systematic geometrical pattern as suggested by Cifuentes et al. (2014a). A total of 9 scans, matching the location of HP measurements, were taken per forest on a 10-m grid within a 20 m × 20 m plot. The used TLS, the FARO® LS880, is a continuous wave laser operating in the near infrared part of the spectrum (λ = 785 nm). It measures the 3D position of objects within a range of 76 m. The continuous output beam emitted from the laser diode passes into the center of a rotating mirror that deflects it to a fixed angle of 90° giving a maximum coverage of 320° on the vertical plane, while a rotating motor allows the 360° azimuth scan. For the present study, the horizontal scanning range was set to full hemispherical coverage and the vertical scanning range was set to 240° to avoid recording unnecessary data from the forest floor. The laser beam was emitted in fixed steps of 0.036° in both the vertical and the horizontal plane. The recorded 3D data were then filtered, registered (i.e., merging of multiple point clouds), classified in green/non-green vegetation, and voxelized.

Filtering and registration

A distance-based filter was applied to the scan points of a single scan re-projected in a 2-dimensional (2D) format. The distance of each scan point (hereafter called pixel when re-projected in 2D) to the sensor was compared to the distance of the pixels located in the adjacent area (i.e., kernel) to the sensor. A kernel represents the shape and size of the neighborhood being sampled (i.e., 3 pixels × 3 pixels square kernel). The pixel being analyzed was removed if, within the kernel, predefined allocation and distance criteria were not fulfilled. The distance-based filter performed an evaluation of each pixel and calculated the amount of pixels within the kernel that are at approximately the same distance from the sensor (i.e., distance threshold) as the pixel being evaluated. The pixel was then classified as valid if a minimum percentage of pixels within the kernel (i.e., allocation threshold) fell within the distance threshold. A detailed description of this filtering procedure for phase-based TLS data can be found in Cifuentes et al. (2014b). Subsequently, reference spheres with known dimensions and reflectivity were used to register the 9-point clouds into 1 comprehensive point cloud dataset, partly overcoming the limitation in range (Van der Zande et al. 2008). A detailed description of the registration procedure for phase-based TLS data can be found in Cifuentes et al. (2014a).

Classification

Classification of point clouds into leaves (i.e., leaves and twigs) and trunks (i.e., trunks and branches) was done in 2 steps. First, subdivision and connection of points from a point cloud using octrees (Jackins and Tanimoto 1980) was performed. The octree algorithm describes a set of 3D data enclosed by a bounding box and outputs sub-clouds of points through the recursive partition of this cubical volume. Each sub-cloud or node in the octree represents the volume formed by a rectangular cuboid, often simplified to an axis aligned cube (Figure 2). An octree node has up to 8 children, each corresponding to 1 octant of the overlying node. Since there is a large degree of coherence between the adjacent cubes in an object, this representation enables a fast projection of all of them into the 3D space (Szeliski 1993). When storing a point cloud, stopping rules for occupied volumes must be defined, for example, a maximal depth (i.e., when recursion has reached a maximum number of sub-division), and a minimal number of points in sub-clouds (Elseberg et al. 2013). The second step was to classify trunks as the sets of sub-clouds where the dimension of their bounding boxes fulfilled minimum height, width, and length requirements. Finally, the remaining sub-clouds were classified as leaves.

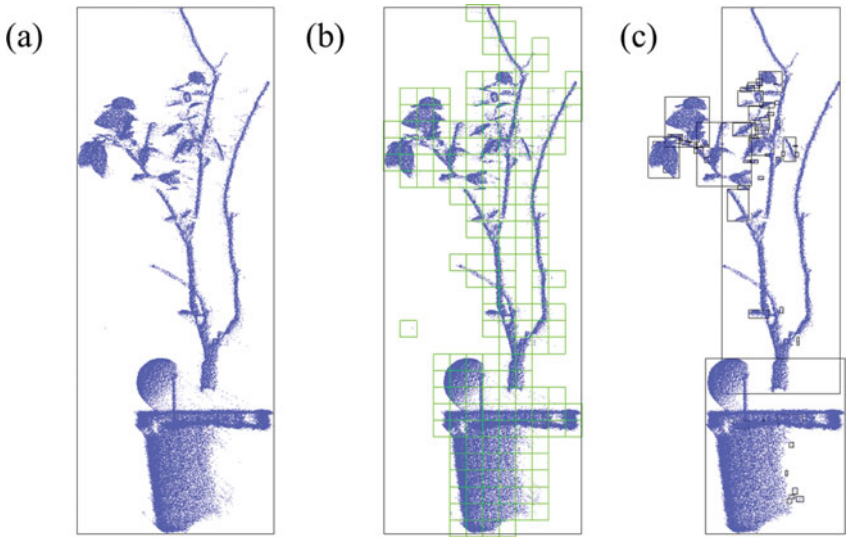

Figure 2. Octree algorithm applied to a sample point cloud (blue dots) visualized in 2D. The point cloud is from a potted orange tree and a reference sphere situated on top of the pot. The initial point cloud enclosed by a black bounding box in (a) is subdivided into cubes represented as green squares in (b). Connected cubes from (b) are then grouped into sub-clouds represented with black bounding boxes in (c), which were later classified into trunks and leaves.

Voxelization

TLS point clouds are characterized by a variable point density in the 3D space due to the angular measurement pattern. For further analysis it is necessary to normalize the point clouds in order to enable comparison of the 3D structure of different parts of the canopy (Van der Zande et al. 2006). A voxel-based approach was used to divide the 3D space into a finite number of cubic voxels, which were classified depending on point/voxel interaction. Voxels with at least 1 return in it were assigned a value of 1 (filled), and a value 0 (empty) was given to voxels that did not enclose any return (Hosoi and Omasa 2007). Prior research on voxel-based canopy reconstruction has concluded that the choice for the optimal voxel size will depend on forest characteristics, the variables under study (e.g., gap fraction distribution, canopy openness), and on the TLS system specifications (Béland et al. 2014; Bittner et al. 2012; Seidel et al. 2012). There is a wide range of voxel sizes recommended in the literature, from where an optimal decision can be deducted. However, a thorough analysis for each specific case is highly advisable. Hence, the present study used cubic voxels with 4 different side lengths for the estimation of canopy structural variables: 10 mm, 20 mm, 26 mm, and 30 mm. At the maximum range of the scanner (76 m), the distance between 2 neighboring beams is 25.75 mm. Thus, using a voxel with a side length of 26 mm will minimize the unsampled space between 2 continuous beams at the maximum range of the instrument.

Models

In ray-tracing environments, a *scene* is defined as the 3D space where the different structures are organized, light sources are specified, and overall rendering parameters (e.g., light transport algorithm or image resolution) are set. An *image*, on the other hand, is the rendered output using the scene description. In this study, these definitions were used for the modeling process, which was performed in 2 stages. The first stage, or *canopy modeling*, used a voxel-based approach to create 3D representations of forest canopies using TLS data, and an analysis of these TLS-derived canopy structures was performed disregarding optical properties of canopy elements. Persistence of Vision Raytracer (POV-Ray; Persistence of Vision Pty. Ltd. 2004) was used to this aim, assessing the quality of the TLS data and defining the optimal voxel size to build the 3D model for the next stage. In the second stage, or light modeling, the optical properties of the different objects were added to the 3D model, for the assessment of PAR transmitted through the canopy (PAR_t) using the physically-based ray tracer (PBRT; Pharr and Humphreys, 2004). Reference leaf reflectance spectra were measured during the field campaign using a FieldSpec® 3 plant probe and leaf clip with the black background panel (Stuckens et al. 2009b). Similarly, reference spectra were measured from trunks and branches (spectral data not presented).

Canopy modeling

POV-Ray allowed to use the full TLS dataset since parameterization is mainly focused on graphical display. Voxels of 4 different sizes were used to build the forest scenes in POV-Ray. The voxels were represented as dark-solid non-reflective cubic objects with white background and no source of light, as in Cifuentes et al. (2014a). For hemispherical image simulation, a virtual fisheye camera with

adjustable field of view was placed on the 9 positions of the 10-m grid. Simulated hemispherical images were rendered, analyzed, and compared with reference HP. The 3 variables under study are detailed hereafter. First, the effective LAI, also referred to as "plant area index" because it includes branches, is a measure of the 1-sided leaf area per unit area (Chen and Black 1991). For leaves that are uniformly distributed with azimuth angle, LAI is defined as

$$\mathrm{LAI} = -\frac{\cos\theta \ln P_0(\theta)}{G(\theta)}, \quad [1]$$

where $P_0(\theta)$ is the gap fraction at an angle θ, and G is the projection of unit area of leaf in the direction θ on a plane perpendicular to that direction. Second, the clumping index (Ω), which indicates the degree of nonrandom distribution of foliage in space (Nilson 1971),

$$\Omega(\theta) = \frac{\ln[F_m(0,\theta)]}{\ln[F_{mr}(0,\theta)]} \cdot \frac{1 - F_{mr}(0,\theta)}{1 - F_m(0,\theta)}, \quad [2]$$

where $F_m(0,\theta)$ is the actual gap size cumulative distribution function along a circular transect at zenith angle θ_i; $F_{mr}(0,\theta)$ is the reduced gap size cumulative distribution function after the largest gaps were removed. The largest gaps are removed iteratively from the tabulated gap dimensions sorted by decreasing values, until differences between successive distributions of gap fractions become negligible. Finally, the CO, which is defined as the proportion of sky hemisphere not obscured by vegetation when viewed from a single point (Jennings et al. 1999),

$$\mathrm{CO} = \sum_{1}^{N} P_0(\varphi,\theta) \cdot [(\cos\theta_1 - \cos\theta_2)/n], \quad [3]$$

where $P_0(\varphi,\theta)$ is the gap fraction in the direction (φ,θ), N is the number of directions given by azimuth and zenith angles ranges, θ_1 is the smallest zenith angle, θ_2 the largest zenith angle of a portion of the hemisphere, and n the number of division of azimuth angles.

Reference and simulated images were processed using CIMES-FISHEYE© (Gonsamo et al. 2011). For LAI and Ω retrievals, image analysis was restricted to view zenith angle ranges (ZAR) 20°–60°, 30°–60°, and 40°–60°, as suggested by various authors and to avoid errors from the lower and higher viewing angles (Gonsamo et al. 2010; Leblanc et al. 2005). All these ZAR included the angle at which the mean projection of leaf area and extinction coefficient are nearly independent of leaf angle distribution (i.e., 57.3°). Additionally, Ω retrievals were as well performed for ZAR 5°–55°, 5°–60°, and 55°–60° as done by García et al. (2015). For CO analysis using voxel-based simulated HP, an appropriate ZAR 0°–30° was defined as a function of the laser scanner maximum range in Seidel et al. (2012). Similarly, ZAR 0°–25°, 0°–30°, and 0°–35° were used for CO retrievals in the present study. After this sensitivity analysis and provided that statistical analysis was completed, the more suitable voxel sizes and ZAR were selected and adopted for reconstructing the 3D models for further light simulations, as detailed in the next section.

Light modeling

The PBRT is a Monte-Carlo rendering system that supports the implementation of different models for light-surface interaction, illumination source, and sensor types. Parameterization in this case is mainly geared towards physiological functioning, limiting the size of the TLS-derived 3D model to be used. A forest scene was built with different components, namely, canopy geometry descriptions, material optical properties, illumination source, sensor platform, and an integrator, which implements the light transport algorithm that computes reflected radiance from surfaces in the scene. Therefore, point assessment of PAR_t was possible once the above mentioned parameters were defined in PBRT. An approach adapted from Stuckens et al. (2009a) was used in this work as is described hereafter.

Canopy geometry description. In order to estimate light transmission using PBRT, the structure of each forest was reconstructed based on the TLS data. Trunks were built as triangular meshes by applying the ball pivoting algorithm described by Bernardini et al. (1999). Similar to the voxel-based light interception model introduced by Van der Zande et al. (2011), leaf voxels were abstracted by triangles with fixed areas from 100 mm^2 to 900 mm^2, depending on the selected voxel side length (Figure 3). The azimuth of the leaves was set randomly and the zenith angle was fixed to the average zenith angle of the dominant tree species (i.e., 42.5° for beech). The extension of the simulated 3D forests were limited to a reference box, which dimensions were defined in function of the zenith angle range selected through canopy modeling and the respective forest mean height, assuring plot-level representativeness of the canopy structure. To render a more realistic forest environment for PAR_t retrievals, 24 instances (or clones) of the reference box were added into the scene as a buffer zone, creating a homogeneous forested area of 150 m × 150 m.

Material optical properties and scene illumination. For tree leaves, a bidirectional scattering distribution function model was used consisting of (*i*) an implementation of a microfacets model to simulate the reflectance of leaves (Bousquet et al. 2005), (*ii*) a Lambertian component for the diffuse reflectance, (*iii*) Lambertian transmittance, and (*iv*) different optical properties for upper and

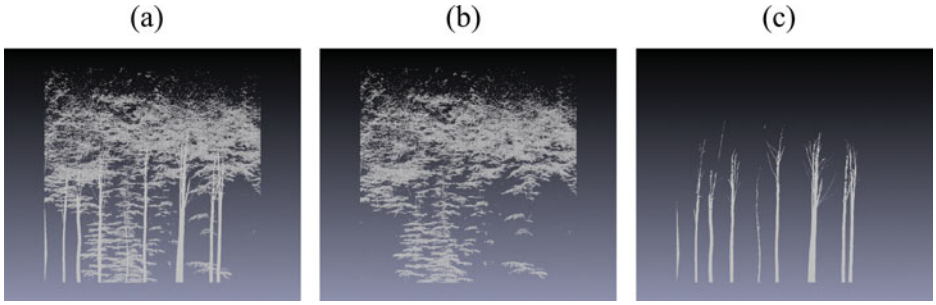

Figure 3. Reconstruction of beech forest stand. The triangular leaves (individual leaf area = 400 mm^2) and the triangular meshes of trunks (a), only leaves (b), and only trunks (c). Objects are shown starting from 2.1 m in height. Orthographic projections generated in Meshlab (Visual Computing Lab–ISTI–CNR, Italy).

back sides of leaves. For trunks, 1 measured spectrum and a Lambertian reflectance model was used (Stuckens et al. 2009a).

For PAR_t simulation, a directional light source and a skymap containing the angular distribution of diffuse light were used to simulate the scene illumination (Figure 4). Direct illumination was calculated as the total direct downward flux at ground altitude (i.e., at 2.1 m above ground), while diffuse illumination was calculated for the entire hemisphere in steps of 2° and 1° in azimuth and zenith angle, respectively.

Sensor platform. In order to simulate the RCR foreoptic, a hyperspectral sensor with spectral range from 400 nm to 700 nm and 10 nm spectral resolution was specified in PBRT. The scenario simulations used a fisheye camera with 180° field of view, in which outputs are expressed as radiance units (W m^{-2} μm^{-1} sr^{-1}). For comparison purposes, the virtual camera was placed over the scene on every cross point of a 1-m grid, at approximately the same location as the below canopy sampling of global irradiance specified earlier.

Simulated PAR_t calculation

A total of 441 hemispherical images per forest were rendered in PBRT, and a cosine correction was applied to each image, enabling measurement of simulated light from the 180° hemisphere. The simulated PAR_t (W m^{-2}) was then calculated at each image, via integration of the adjusted radiance values in the 400 nm–700 nm range using the Trapezoid Rule (Whittaker and Robinson 1924). This case was given by the formula:

$$A = \frac{\Delta x}{2}((y_0) + 2(y_1) + 2(y_2) + \cdots + 2(y_{n-1}) + (y_n)), \quad [4]$$

where A is the approximate area under the curve between 400 nm and 700 nm (i.e., the PAR_t value),

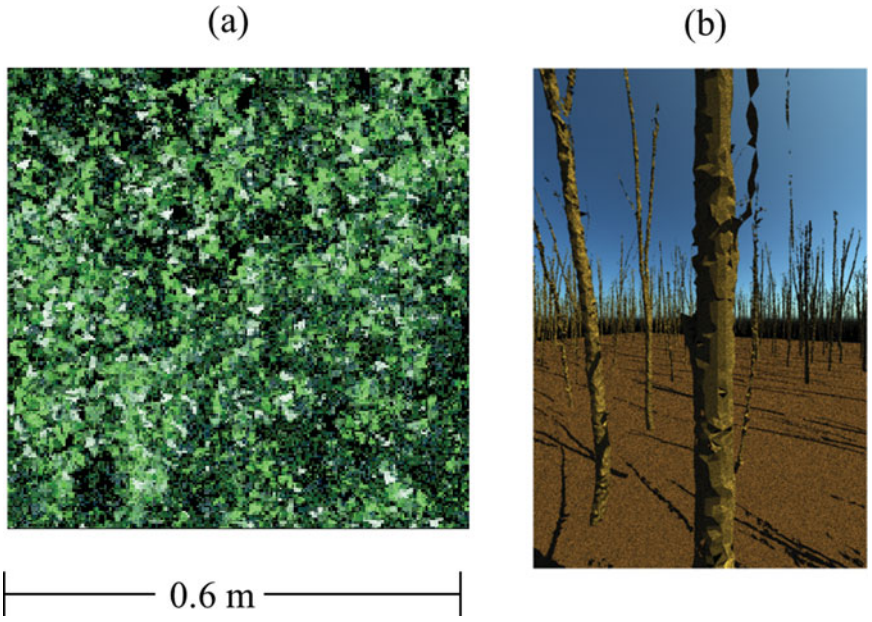

Figure 4. Detailed orthogonal view from top of canopy (a) and perspective view of a trunk section from a leaf-off image (b). Triangular canopy leaves are shown in green, trunks and soil in brown, and sky map in blue. Images were rendered in PBRT.

Δx is the trapezoid height, n is the number of trapezoids, and y is the measured radiance value (i.e., trapezoid width). For a better understanding of the relationship between simulated and observed photosynthetically active radiation transmitted through the canopy ($sPAR_t$ and $oPAR_t$, respectively), both $sPAR_t$ and $oPAR_t$ values were scaled to range between 0 and 1 as $(sPAR_t)scaled = [sPAR_t - (sPAR_t)_{min}]/[(sPAR_t)_{max} - (sPAR_t)_{min})]$ and $(oPAR_t)scaled = [oPAR_t - (oPAR_t)_{min}]/[(oPAR_t)_{max} - (oPAR_t)_{min})]$, where subscripts min and max define minimal and maximal values of $sPAR_t$ and $oPAR_t$.

Statistical analysis

Comparisons between observed and TLS-derived simulated values of a number of variables have been generally performed using the coefficient of determination (R^2), a statistical measure of how close the data are to the fitted regression line. See, for example, the use of R^2 for these comparisons in works by Holopainen et al. (2011), Moorthy et al. (2008), Seidel et al. (2012), Vaccari et al. (2013), and Van Leeuwen and Nieuwenhuis (2010). This coefficient does provide an estimate of the strength of the relationship between the model and the response variable; however, it does not provide a formal hypothesis test for this relationship. In order to assess the relationship between observed and simulated variables from the 3D model (i.e., LAI, Ω, CO, and PAR_t), a linear regression model was fit and evaluated placing observed values in the ordinates and simulated values in the abscissas as recommended in Piñeiro et al. (2008). Furthermore, we tested the hypotheses of $\beta_0 = 0$ and $\beta_1 = 1$, and confidence intervals were calculated ($\alpha = 0.01$) to statistically assess the significance of regression coefficients for the studied variables. If the null hypothesis for the slope is rejected, the conclusion is that simulations have no consistency with observed values. If this hypothesis is not rejected but the hypothesis for the intercept is, then the model is biased. If both null hypotheses are not rejected, then disagreement between model predictions (i.e., simulated values) and observed data is due entirely to the unexplained variance. Besides, the root mean squared deviation (RMSD) was calculated for each variable being simulated, representing the mean deviation of simulated values in relation to the observed ones (Kobayashi and Salam 2000).

Results

Foliage at higher parts of the canopy was only partially represented due to occlusion issues when collecting the TLS data (Figure 3). The sparse leaves distributed randomly in the upper parts represent only a proportion of the real forest canopy or tree crown. Lower vegetation, however, appears to be well displayed. Similarly, some trunks and branches were not fully represented, therefore, only segments of trunks were created using the meshing algorithm in the voxelized space. This condition occurred mainly at higher levels in the canopy in both forest stands. This inherent limitation of TLS systems in representing the top of the canopy will probably influence further processing steps, such as light modeling, and consequently, impact in the simulation results. Reference HP and simulated HP from POV-Ray are presented in Figure 5. Objects like trunks, branches, and nearby foliage were clearly detectable from both images. Canopy gaps near zenith were also identifiable, but objects and gaps (and their patterns) are less definite at higher zenith angles in the simulated HP, as the 3D position of elements located further from 76 m from measuring points are not recorded by the FARO® LS880.

Regarding the canopy structure analysis, simulated values of LAI, Ω, and CO were compared to observed values

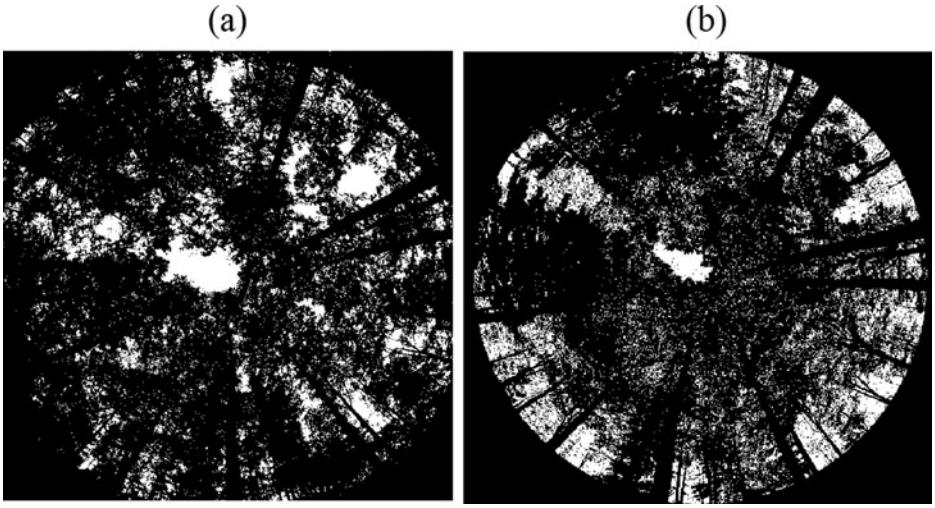

Figure 5. Real (a) and simulated (b) B/W hemispherical photographs from the beech forest. Image (b) was rendered in POV-Ray.

Table 1. Estimated parameters ($\hat{\beta}_0$, $\hat{\beta}_1$) for each variable being simulated depending on the selected zenith angle ranges (ZAR) and voxel sizes in each forest type. Their respective proportion of variation (R^2) and root mean squared deviation (*RMSD*) are presented.

Forest	Variable	ZAR (°)	Voxel Size (mm)	$\hat{\beta}_0$	$\hat{\beta}_1$	R^2	*RMSD* (%)
Mixed	LAI	30–60	10	0.109	1.138	0.50	20.0
	Ω	55–60	10	− 2.344	3.327	0.27*	9.8
	CO	5–35	10	0.017	0.606	0.41	30.0
Beech	LAI	20–60	20	0.641	0.738	0.70	8.3
	Ω	5–55	20	− 0.933	1.795	0.76	26.0
	CO	5–25	20	− 0.002	1.271	0.44	30.0

*Not considered for further analysis.

and the significance of the intercept ($\hat{\beta}_0$) and slope ($\hat{\beta}_1$) were tested. Regressions with an R^2 lower than 0.4 were excluded from further analysis.

For LAI in mixed forest, hypothesis testing confirmed that at ZAR 30°–60°, neither of the null hypotheses (i.e., $\beta_0 = 0$ and $\beta_1 = 1$) can be rejected when using both 10 mm ($R^2 = 0.5$ and $RMSD = 20\%$) and 20 mm ($R^2 = 0.5$ and $RMSD = 27\%$) voxel size. The same is true for beech forest using voxel size 20 mm at ZAR 20°–60°, with $R^2 = 0.7$ and $RMSD = 8.3\%$.

Hypothesis testing for Ω established that in a mixed forest neither of the null hypotheses can be rejected at all ZAR using the whole range of voxel sizes. R^2, however, presented very low values in all regressions with a maximum $R^2 = 0.27$ ($RMSD = 9.8\%$) using voxel size 10 mm at ZAR 55°–60°. For beech forest, in turn, this scenario (i.e., voxel size 10 mm, ZAR 55°–60°) was the only one where null hypotheses were rejected ($R^2 = 0.22$ and $RMSD = 10\%$). On the contrary, using larger voxel sizes and greater ZAR delivered the higher R^2. At ZAR 5°–55° and 5°–60° using voxel sizes 20 mm, 26 mm, and 30 mm, the R^2 values were all greater than 0.6, with a maximum $R^2 = 0.76$ ($RMSD = 26\%$) using voxel size 20 mm at ZAR 5°–55°.

For CO retrievals in the mixed forest neither of the null hypotheses can be rejected using voxel size 10 mm at all ZAR ($R^2 > 0.41$, $RMSD < 30\%$). For beech forest, the null hypothesis for the slope is only rejected using voxel size 10 mm in the 0°–35° ZAR, all other scenarios have $R^2 > 0.41$ and $RMSD < 45\%$.

The canopy structure analysis confirmed that there is more than 1 suitable voxel size and zenith angle range for 3D model construction. Using this information, the next step is the reconstruction of the forest scene in PBRT for light simulation and PAR_t assessment. Table 1 displays a summary of regression results for each of the structural variables per forest type.

As described above, the selected voxel sizes were identical for all 3 variables within forest type. The ZAR in turn, were slightly different for LAI and CO. Given the high memory costs in processing ray-tracing algorithms, the 3D space to be created in PBRT was defined as a 30 × 30 m plot at both mixed and beech forest. Tree tops located at plot edges (i.e., 15 m from center of plot), intersected with the maximum zenith angle of ZAR for better CO estimates (i.e., mixed: 35°; beech: 25°). The extent of this 3D space was defined as a compromise between 2 criteria: it should include the lower zenith angles (i.e., where a high coverage of the 3D space is acquired), being large enough so most canopy elements and all irradiance measurements are included; but compact enough to efficiently process ray-tracing algorithms.

The PAR_t retrieved below forest canopies was simulated using the attributes selected in the previous section. For the mixed forest a voxel size 10 mm and ZAR 0°–35° was used, while voxel size 20 mm and ZAR 0°–25° was applied for beech forest. Figure 6b shows an image with the 3D model from the phase-based TLS data added to the PBRT scene, implementing the cited parameters and incorporating the illumination source. For comparison, Figure 6a shows a real beech stand at Heverlee Forest.

The mean difference between scaled $oPAR_t$ and $sPAR_t$ and its variability is higher at lower values and tends to decrease at elevated values of PAR_t in mixed forest. Similarly, a higher difference and variability is seen at $PAR_t < 0.1$ in the beech forest. In the latter case, however, mean differences are lower and more stable at elevated values of PAR_t (Figure 7).

Simple linear regression of PAR_t delivered slopes < 1 and intercepts > 0 on both forests (Table 2). The points of intersection with the 1:1 line are between 0.4–0.45 on mixed forest, and between 0.45–0.5 on beech forest, meaning that below these points simulated values underestimated PAR_t, above them, simulated values overestimated PAR_t.

Table 2. Estimated parameters ($\hat{\beta}_0$, $\hat{\beta}_1$), proportion of variation (R^2), and root mean squared deviation (*RMSD*) for simulated transmitted photosynthetically active radiation (PAR_t) in mixed and beech forest stands.

Forest	$\hat{\beta}_0$	$\hat{\beta}_1$	R^2	*RMSD* (%)
Mixed	0.20134	0.58484	0.1729	35.9
Beech	0.15991	0.64212	0.4702	33.1

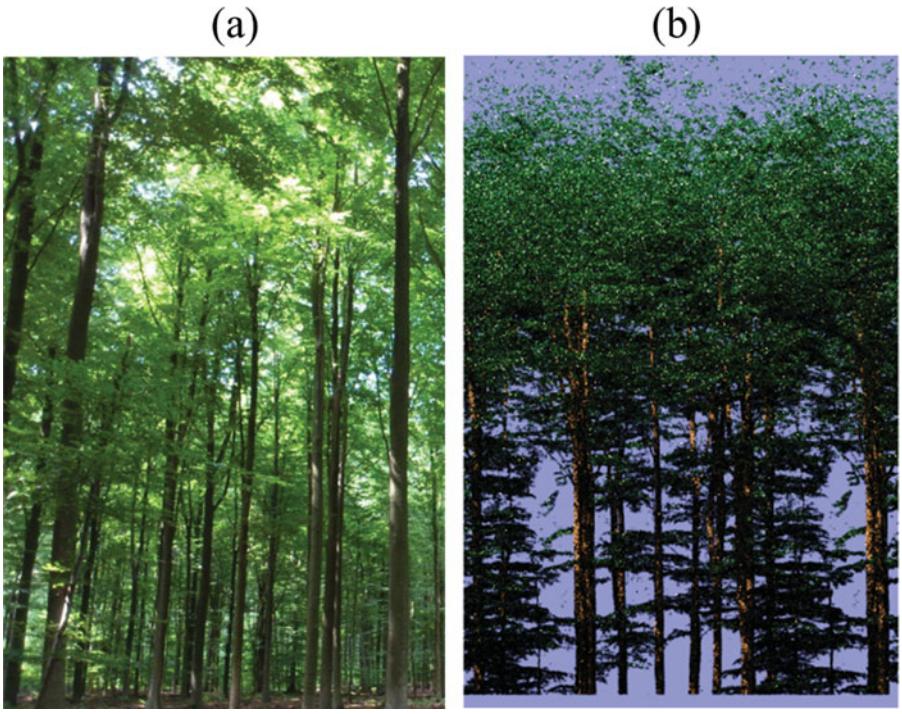

Figure 6. Real beech forest at the Heverlee Forest (a) and RGB composite image of the modeled beech forest (b). Image (b) was rendered with orthographic projection in PBRT.

Discussion

POV-Ray simulations of HP provides a first visual assessment of similarities and differences between the real and simulated forests (Figure 5). Site specific parameters, such as spectral properties of canopy elements, leaf size, and branching architecture, govern interactions between laser pulses and canopy elements impacting the realism of TLS-derived 3D models. Other issues linked to the TLS technology, such as laser beam divergence, ghost points, and scan resolution, can also explicate these differences (Pueschel et al. 2014). Furthermore, occluded areas contribute to systematic biases in estimates, especially in dense forests. Registration of multiple point clouds delivers a comprehensive 3D data set, nevertheless occlusion effects remain an important factor and can significantly alter canopy structure estimates using 3D models of dense canopies (Béland et al. 2014).

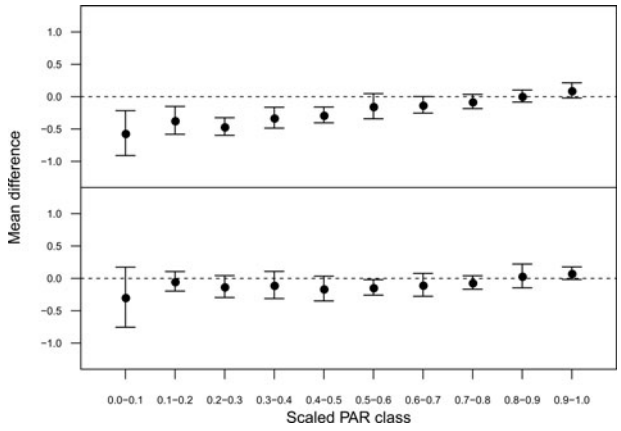

Figure 7. Mean difference between scaled observed PAR_t vs. scaled simulated PAR_t per class in the mixed (top) and beech (bottom) forest. Error bars represent the standard deviation.

TLS-derived 3D models have been used in previous analyses of vegetation structure, estimating forest canopy gap fraction (Ramirez et al. 2013), leaf area and biomass of individual trees (Holopainen et al. 2011; Huang and Pretzsch 2010), and canopy openness (Seidel et al. 2012), using point-, intensity-, and voxel-based approaches. The latter method was found to be suitable for simulating HP from phase-based LiDAR data, and inefficiently create objects for light simulations. However, voxel size cannot be defined a priori, hence, sensitivity analyses were performed. Results after hypothesis testing demonstrated that for every canopy structure variable, better simulated values were computed using voxel size 10 mm in mixed forest and voxel size 20 mm in beech forest. These findings differ from the findings of Cifuentes et al. (2014a), where gap fractions at similar forest types were better simulated using larger voxel sizes at ZAR 0°–70°.

Selecting an appropriate voxel size for canopy structure assessments appears to be conditioned by the objective of the study. It has been found, for instance, that voxels size of 10 times the leaf size were appropriate to study single-tree 3D foliage distribution and to derive spatially explicit estimates (Béland et al. 2014). In this case, using a voxel

size larger than the laser pulse cross section, helped in dealing with occlusion effects. On the other hand, realistic 3D models of forested environments and canopy structure have been reconstructed using smaller voxel sizes, e.g., 10 mm, 20 mm, 30 mm, and 100 mm (Bittner et al. 2012; Cifuentes et al. 2014a; Seidel et al. 2012; Van der Zande et al. 2008). In conclusion, either when deriving leaf area within the space of a geometric volume or for emulating reality for canopy structure assessment and light simulation, the size of the volume needs to be carefully chosen as it can impact canopy structure estimates. This influence can be seen for LAI and CO estimates in Figures 5 and 7, respectively. In agreement with the findings of Béland et al. (2014), increasing voxel sizes delivered decreasing observed values of LAI (when LAI > 2).

This study performed canopy assessments within restricted zenith angle ranges (e.g., 20° to 60° for LAI, 5° to 60° for Ω, and 0° to 35° for CO), minimizing the impact of erroneous estimates of structural variables (Gonsamo and Pellikka 2009). However, as reported by Leblanc et al. (2005) and Weiss et al. (2004), the information of canopy structure retrieved from zenith angles larger than 60° is relevant for further analysis of, for example, LAI, leaf area distribution, or foliage profiles. Hence, possible issues with canopy structure estimates at zenith angles larger than 60° need to be further studied.

Previous studies have used registered TLS data to validate incremental segmentation algorithms for point cloud segmentation using octrees (Wang and Tseng 2011). Their approach efficiently segmented TLS point clouds of curved surfaces using adaptive proximity and coherence criteria to form co-surface points after merging neighboring coplanar points. An octree-based space division procedure is also used in the CAMPINO (collapsing and merging procedures in octree-graphs) method designed for hard targets (i.e., planes and curved surfaces) allowing for geometric tree skeleton reconstructions (Bucksch and Lindenbergh 2008). Although, it has been demonstrated that separating leaves and trunks improves the estimation of relevant canopy structure variables, such as LAI (Moorthy et al. 2008), the uneven spacing of the TLS point cloud may lead to segmentation errors and, therefore, inadequate classification especially on data collected under dense forest canopies.

Applying the selected voxel size for efficiently representing 3D canopies, we were able to simulate light conditions (PAR_t) near the forest floor within the same ranges as observed values (Figure 7). The differences between mixed and beech forest (RMSD of 35% and 33%, respectively; Table 2) can be explained by the increased occlusion effect on denser forests. Similar differences have been reported in Van der Zande et al. (2011) for leaf area density estimates on virtual forests. After correcting for these percentage differences and perform hypothesis testing, is was not possible to reject the null hypothesis for the slope ($\beta_1 = 1$), meaning that simulations are consistent with observed values. Simulations were biased, due to rejection of null hypothesis for the intercept ($\beta_0 = 0$) in both forest types.

Point to point comparison delivers low correlation coefficients of 0.17 and 0.47 for mixed and beech forest, respectively. High variability in both in situ measurements and simulations, can be associated to the heterogeneous arrangement of canopy elements in irregular or mixed forest stands (Courbaud et al. 2003; Giuliani and Brown 2008). Further reasons to explain this behavior can be related to, first, atmospheric conditions (e.g., differences between reference and below canopy radiation records), given that direct validation did not yield good results given the extent of separation between the instruments (1.7 km). Second, 3D model construction, since TLS limitations to scan the top of canopy (Figure 6) and the mentioned occlusion effect can influence 3D models and light simulation. Adding simulated biomass in the upper layers based on the structure measured in lower layers can be an option to minimize this constraint. Another option is to incorporate 3D data from airborne LiDAR or taking advantage of the rapidly increasing technology of unmanned aerial vehicles (UAV). The latter can be used to collect data at different heights, providing a solution and valuable 3D data on the location of foliage elements that are embedded in the canopy (Chisholm et al. 2013). Finally, parameterization of PBRT, given that a grid of 1 m × 1 m (or any other dimension) was perfectly outlined within the ray-tracing environment. Real measurements, however, were conditioned by topography and location of trees, where mismatch between the positions of the simulated sensor versus the real locations were noted. As confirmed by Bittner et al. (2012) on their study about PAR measured under an experimental beech stand and controlled conditions, small variations of the sensor position (e.g., close to trunks, branches, or leaves), may lead to significant variations of the recorded values. A spatial point to point comparison approach generally shows reduced agreement caused by small errors in crown location (Mariscal et al. 2004). Assumptions in 3D forest canopy reconstruction for light modeling could have also contributed to the low correlation between observed and simulated values of PAR_t. For example, although including several instances of the central block allowed to count for lateral radiation fluxes, it may have also influenced the results in PAR_t simulation by "closing" gaps that existed in the real forest stands (i.e., outside the 30 m × 30 m central block).

With regard to the PBRT scene description, parameters and their values used to represent the objects, other

techniques may be explored in order to make the rendering process more efficient. For example, the duplication of the central instance to avoid the problem of low elevation angles can be replaced for an alternative, as shown in Da Silva et al. (2012), with the addition of a wall with calibrated opacity representing the radiative properties of the environment and saving computing time. Using this wall, however, will render unrealistic forest scenes, adding limitations for reliably computing incoming irradiance along a vertical or horizontal gradient.

We firmly believe that if proper actions are taken in order to minimize these errors and improve performance, it will be possible to better simulate canopy-light interactions at different height levels within the forest canopy.

Unlike 3D models derived from airborne laser scanning data, which will deliver more accurate representation of tree tops (Chasmer et al. 2006; Falkowski et al. 2008), the presented approach seems to be appropriate to characterize understory and forest structure at lower height classes. According to Disney et al. (2006), the understory is likely to influence the top-of-canopy signal at young ages and/or stands of low density, reducing sensitivity of the measured signal. Thus, the use of more realistic description of the understory, such as the presented 3D models from TLS data, may improve the sensitivity of the modeled signal from the top of canopy. This was not the aim of the present study, thus the analysis of, for example, influence of canopy structure on top-of-canopy signal is a matter of future investigation.

Conclusions

Phase-based TLS data allowed to build proper 3D canopy models for structural characterization of 2 types of forests, providing important inputs for canopy-light interaction analysis in a ray-tracing environment. The hypotheses testing based on an observed-predicted regression model is shown to be suitable for modeling canopy structure, allowing to test several variables in different settings, and providing a statistical framework for assessing the uncertainty of relationships between observed and simulated variables. Although limitation in range is reduced by registering point clouds, it is still a major issue for some TLS systems. Registration also minimizes occlusion effects, but this issue will also depend on vegetation, forest stand, and understory characteristics. Nevertheless, it was demonstrated that assessments of canopy structural variables using voxel-based 3D models from real forests were comparable to observed ones, at specific zenith angle ranges. Classification using octrees was a key step for adequate simulation of canopy-light interactions, helping to overcome the limitation of the monochromatic TLS in clustering points together as leaves or trunks. Although the 3D models accounted for tree clump and large gaps, as well as for small gaps within the tree crowns, low correlations were observed in point to point examinations of PAR_t. The mean differences between observed and simulated PAR_t values in the mixed forest are larger than in the beech forest. These differences can be associated with several factors including the mentioned elevated occlusion in dense heterogeneous forests, atmospheric conditions, 3D model construction, and parameterization for ray tracing.

The results of this study demonstrated the potential of TLS data to create forest canopy models that can be used for light modeling, as well as currently unresolved issues. To improve 3D space sampling procedures, it is recommended to explore the use of UAVs for scanning forest canopies at different height levels. Moreover, sensitivity analyses can be performed in order to identify the optimal features for canopy reconstruction, e.g., the impact of leaf angle, shape, and size in light distribution simulations. This information complemented with within-canopy radiation data, can be useful to fully characterize the canopy structure, estimate canopy growth, and to predict natural or managed forest renovation and model forest succession. 3D models and light simulations can then be adjusted, tested, and extended to handle the full electromagnetic spectrum of incoming radiation. Thus, improved functional-structural models of forests can be used to the estimation of, for example, energy fluxes inside the canopy and between canopy elements and forest floor. A combined structural and radiometric modeling approach is recommended in order to explore the impact of canopy structure on the resulting remotely sensed signal. Future work could also incorporate airborne LiDAR and hyperspectral data in order to quantify this impact at both local and landscape scale.

Acknowledgments

We would like to thank the Flemish-Brabant Agency for Nature and Forest for the willingness to contribute to this research. Special thanks go to Wanda De Keersmaecker, Jonathan Van Beek, José Miguel Barrios, and Raymond Struthers for their valuable assistance during field campaigns.

Funding

Funding support for this study has been provided by the HYPERFOREST project (SR/00/134).

References

Ågren, G.I., McMurtrie, R.E., Parton, W.J., Pastor, J., and Shugart, H.H. 1991. "State-of-the-art of models of production-decomposition linkages in conifer and grassland ecosystems." *Ecological Applications*, Vol. 1: pp. 118–138.

Béland, M., Baldocchi, D.D., Widlowski, J.-L., Fournier, R.A., and Verstraete, M.M. 2014. "On seeing the wood from the leaves and the role of voxel size in determining leaf area distribution of forests with terrestrial LiDAR." *Agricultural and Forest Meteorology*, Vol. 184: pp. 82–97. doi: 10.1016/j.agrformet.2013.09.005

Belton, D., and Lichti, D.D. 2006. "Classification and segmentation of terrestrial laser scanner point clouds using local variance information." *ISPRS—International Archives of the Photogrammetry, Remote Sensing and Spatial Information Sciences*, Vol. 38(No. 5): pp. 44–49.

Bernardini, F., Mittleman, J., Rushmeier, H., Silva, C., and Taubin, G. 1999. "The ball-pivoting algorithm for surface reconstruction." *IEEE Transactions on Visualization and Computer Graphics*, Vol. 5: pp. 349–359.

Bittner, S., Gayler, S., Biernath, C., Winkler, J.B., Seifert, S., Pretzsch, H., and Priesack, E. 2012. "Evaluation of a ray-tracing canopy light model based on terrestrial laser scans." *Canadian Journal of Remote Sensing*, Vol. 38: pp. 619–628.

Bousquet, L., Lachérade, S., Jacquemoud, S., and Moya, I. 2005. "Leaf BRDF measurements and model for specular and diffuse components differentiation." *Remote Sensing of Environment*, Vol. 98: pp. 201–211. doi: 10.1016/j.rse.2005.07.005

Bucksch, A., and Lindenbergh, R. 2008. "CAMPINO—A skeletonization method for point cloud processing." *ISPRS Journal of Photogrammetry and Remote Sensing*, Vol. 63: pp. 115–127. doi: 10.1016/j.isprsjprs.2007.10.004

Cescatti, A. 1997. "Modelling the radiative transfer in discontinuous canopies of asymmetric crowns. I. Model structure and algorithms." *Ecological Modelling*, Vol. 101: pp. 263–274. doi: 10.1016/S0304-3800(97)00050-1

Chasmer, L., Hopkinson, C., and Treitz, P. 2006. "Investigating laser pulse penetration through a conifer canopy by integrating airborne and terrestrial lidar." *Canadian Journal of Remote Sensing*, Vol. 32: pp. 116–125. doi: 10.5589/m06-011

Chen, J.M., and Black, T.A. 1991. "Measuring leaf area index of plant canopies with branch architecture." *Agricultural and Forest Meteorology*, Vol. 57: pp. 1–12.

Chisholm, R.A., Cui, J., Lum, S.K.Y., and Chen, B.M. 2013. "UAV LiDAR for below-canopy forest surveys." *Journal of Unmanned Vehicle Systems*, Vol. 1: pp. 61–68. doi: 10.1139/juvs-2013-0017

Cifuentes, R., Van der Zande, D., Farifteh, J., Salas, C., and Coppin, P. 2014a. "Effects of voxel size and sampling setup on the estimation of forest canopy gap fraction from terrestrial laser scanning data." *Agricultural and Forest Meteorology*, Vol. 194: pp. 230–240. doi: 10.1016/j.agrformet.2014.04.013

Cifuentes, R., Van der Zande, D., Salas, C., Farifteh, J., and Coppin, P. 2014b. "Correction of erroneous LiDAR measurements in artificial forest canopy experimental setups." *Forests*, Vol. 5: pp. 1565–1583. doi: 10.3390/f5071565

Côté, J.-F., Fournier, R.A., and Egli, R. 2011. "An architectural model of trees to estimate forest structural attributes using terrestrial LiDAR." *Environmental Modelling & Software*, Vol. 26: pp. 761–777. doi: 10.1016/j.envsoft.2010.12.008

Côté, J.-F., Widlowski, J.-L., Fournier, R., and Verstraete, M. 2009. "The structural and radiative consistency of three-dimensional tree reconstructions from terrestrial lidar." *Remote Sensing of Environment*, Vol. 113: pp. 1067–1081. doi: 10.1016/j.rse.2009.01.017

Courbaud, B., de Coligny, F., and Cordonnier, T. 2003. "Simulating radiation distribution in a heterogeneous Norway spruce forest on a slope." *Agricultural and Forest Meteorology*, Vol. 116: pp. 1–18. doi: 10.1016/S0168-1923(02)00254-X

Da Silva, D., Balandier, P., Boudon, F., Marquier, A., and Godin, C. 2012. "Modeling of light transmission under heterogeneous forest canopy: An appraisal of the effect of the precision level of crown description." *Annals of Forest Science*, Vol. 69: pp. 181–193. doi: 10.1007/s13595-011-0139-2

Danson, F.M., Gaulton, R., Armitage, R.P., Disney, M., Gunawan, O., Lewis, P., Pearson, G., and Ramirez, A.F. 2014. "Developing a dual-wavelength full-waveform terrestrial laser scanner to characterize forest canopy structure." *Agricultural and Forest Meteorology*, Vol. 198–199: pp. 7–14. doi: 10.1016/j.agrformet.2014.07.007

Dassot, M., Colin, A., Santenoise, P., Fournier, M., and Constant, T. 2012. "Terrestrial laser scanning for measuring the solid wood volume, including branches, of adult standing trees in the forest environment." *Computers and Electronics in Agriculture*, Vol. 89: pp. 86–93. doi: 10.1016/j.compag.2012.08.005

Dassot, M., Constant, T., and Fournier, M. 2011. "The use of terrestrial LiDAR technology in forest science: Application fields, benefits and challenges." *Annals of Forest Science*, Vol. 68: pp. 959–974. doi: 10.1007/s13595-011-0102-2

Demantké, J., Mallet, C., David, N., and Vallet, B. 2011. "Dimensionality based scale selection in 3D LiDAR point clouds." *ISPRS—International Archives of the Photogrammetry, Remote Sensing and Spatial Information Sciences*, Vol. 38: pp. 97–102. doi: 10.5194/isprsarchives-XXXVIII-5-W12-97-2011

Disney, M., Lewis, P., and Saich, P. 2006. "3D modelling of forest canopy structure for remote sensing simulations in the optical and microwave domains." *Remote Sensing of Environment*, Vol. 100: pp. 114–132. doi: 10.1016/j.rse.2005.10.003

Disney, M.I., Kalogirou, V., Lewis, P., Prieto-Blanco, A., Hancock, S., and Pfeifer, M. 2010. "Simulating the impact of discrete-return lidar system and survey characteristics over young conifer and broadleaf forests." *Remote Sensing of Environment*, Vol. 114: pp. 1546–1560. doi: 10.1016/j.rse.2010.02.009

Easter, M.J., and Spies, T.A. 1994. "Using hemispherical photography for estimating photosynthetic photon flux density under canopies and in gaps in Douglas-fir forests of the Pacific Northwest." *Canadian Journal of Forest Research*, Vol. 24: pp. 2050–2058.

Elseberg, J., Borrmann, D., and Nüchter, A. 2013. "One billion points in the cloud—An octree for efficient processing of 3D laser scans." *ISPRS Journal of Photogrammetry and Remote Sensing*, Vol. 76: pp. 76–88. doi: 10.1016/j.isprsjprs.2012.10.004

Falkowski, M.J., Smith, A.M.S., Gessler, P.E., Hudak, A.T., Vierling, L.A, and Evans, J.S. 2008. "The influence of conifer forest canopy cover on the accuracy of two individual tree measurement algorithms using lidar data." *Canadian Journal of Remote Sensing*, Vol. 34: pp. S338–S350. doi: 10.5589/m08-055

García, M., Gajardo, J., Riaño, D., Zhao, K., Martín, P., and Ustin, S. 2015. "Canopy clumping appraisal using terrestrial and airborne laser scanning." *Remote Sensing of Environment*, Vol. 161: pp. 78–88. doi: 10.1016/j.rse.2015.01.030

Gendron, F., Messier, C., Lo, E., and Comeau, P.G. 2006. "The angular distribution of diffuse photosynthetically active radiation under different sky conditions in the open and within deciduous and conifer forest stands of Quebec and British Columbia, Canada." *Annals of Forest Science*, Vol. 63: pp. 43–53. doi: 10.1051/forest

Giuliani, R., and Brown, K.J. 2008. "Within-canopy sampling of global irradiance to describe downwelling light distribution and infer canopy stratification in a broadleaf forest." *Tree Physiology*, Vol. 28: pp. 1407–1419.

Gobron, N., and Verstraete, M.M. 2009. *ECV T10: Fraction of Absorbed Photosynthetically Active Radiation (FAPAR)*. Rome, Italy: Food and Agriculture Organization of the United Nations.

Gonsamo, A., and Pellikka, P. 2009. "The computation of foliage clumping index using hemispherical photography." *Agricultural and Forest Meteorology*, Vol. 149: pp. 1781–1787. doi: 10.1016/j.agrformet.2009.06.001

Gonsamo, A., Walter, J.-M.N., and Pellikka, P. 2010. "Sampling gap fraction and size for estimating leaf area and clumping indices from hemispherical photographs." *Canadian Journal of Forest Research*, Vol. 40: pp. 1588–1603. doi: 10.1139/X10-085

Gonsamo, A., Walter, J.-M.N., and Pellikka, P. 2011. "CIMES: A package of programs for determining canopy geometry and solar radiation regimes through hemispherical photographs." *Computers and Electronics in Agriculture*, Vol. 79: pp. 207–215. doi: 10.1016/j.compag.2011.10.001

Hardy, J.P., Melloh, R., Koenig, G., Marks, D., Winstral, A., Pomeroy, J.W., and Link, T. 2004. "Solar radiation transmission through conifer canopies." *Agricultural and Forest Meteorology*, Vol. 126: pp. 257–270. doi: 10.1016/j.agrformet.2004.06.012

Hilker, T., Leeuwen, M., Coops, N.C., Wulder, M.A., Newnham, G.J., Jupp, D.L.B., and Culvenor, D.S. 2010. "Comparing canopy metrics derived from terrestrial and airborne laser scanning in a Douglas-fir dominated forest stand." *Trees*, Vol. 24: pp. 819–832. doi: 10.1007/s00468-010-0452-7

Holbrook, N.M., and Lund, C.P. 1995. "Photosynthesis in forest canopies." In *Forest Canopies*, edited by M.D. Lowman and N.M. Nadkarni, pp. 411–430. San Diego, CA: Academic.

Holopainen, M., Vastaranta, M., Kankare, V., Räty, M., Vaaja, M., Liang, X., Yu, X., Hyyppä, J., Hyyppä, H., Viitala, R., and Kaasalainen, S. 2011. "Biomass estimation of individual trees using stem and crown diameter TLS measurements." *ISPRS—International Archives of the Photogrammetry, Remote Sensing and Spatial Information Sciences*, Vol. 38: pp. 91–95. doi: 10.5194/isprsarchives-XXXVIII-5-W12-91-2011.

Hopkinson, C., Chasmer, L., Young-Pow, C., and Treitz, P. 2004. "Assessing forest metrics with a ground-based scanning lidar." *Canadian Journal of Forest Research*, Vol. 34: pp. 573–583. DOI: 10.1139/x03-225

Hosoi, F., and Omasa, K. 2007. "Factors contributing to accuracy in the estimation of the woody canopy leaf area density profile using 3D portable lidar imaging." *Journal of Experimental Botany*, Vol. 58: pp. 3463–3473. doi: 10.1093/jxb/erm203

Huang, H., Qin, W., and Liu, Q. 2013. "RAPID: A radiosity applicable to porous individual objects for directional reflectance over complex vegetated scenes." *Remote Sensing of Environment*, Vol. 132: pp. 221–237. doi: 10.1016/j.rse.2013.01.013

Huang, P., and Pretzsch, H. 2010. "Using terrestrial laser scanner for estimating leaf areas of individual trees in a conifer forest." *Trees*, Vol. 24: pp. 609–619. doi: 10.1007/s00468-010-0431-z

Jackins, C., and Tanimoto, S. 1980. "Oct-trees and their use in representing three-dimensional objects." *Computer Graphics and Image Processing*, Vol. 14: pp. 249–270.

Jennings, S.B., Brown, N.D., and Sheil, D. 1999. "Assessing forest canopies and understorey illumination: Canopy closure, canopy cover and other measures." *Forestry*, Vol. 72: pp. 59–73. doi: 10.1093/forestry/72.1.59

Jonckheere, I., Fleck, S., Nackaerts, K., Muys, B., Coppin, P., Weiss, M., and Baret, F. 2004. "Review of methods for in situ leaf area index determination. Part I. Theories, sensors and hemispherical photography." *Agricultural and Forest Meteorology*, Vol. 121: pp. 19–35. doi: 10.1016/j.agrformet.2003.08.027

Jupp, D.L.B., Culvenor, D.S., Lovell, J.L., Newnham, G.J., Strahler, H., and Woodcock, C.E. 2009. "Estimating forest LAI profiles and structural parameters using a ground-based laser called "Echidna"." *Tree Physiology*, Vol. 29: pp. 171–181. doi: 10.1093/treephys/tpn022

Kobayashi, K., and Salam, M.U. 2000. "Comparing simulated and measured values using mean squared desviation and its components." *Agronomy Journal*, Vol. 92: pp. 345–352. doi: 10.1007/s100870050043

Korhonen, L., Korpela, I., Heiskanen, J., and Maltamo, M. 2011. "Airborne discrete-return LIDAR data in the estimation of vertical canopy cover, angular canopy closure and leaf area index." *Remote Sensing of Environment*, Vol. 115: pp. 1065–1080. doi: 10.1016/j.rse.2010.12.011

Law, B., Cescatti, A., and Baldocchi, D. 2001. "Leaf area distribution and radiative transfer in open-canopy forests: implications for mass and energy exchange." *Tree Physiology*, Vol. 21: pp. 777–787.

Leblanc, S.G., Chen, J.M., Fernandes, R., Deering, D.W., and Conley, A. 2005. "Methodology comparison for canopy structure parameters extraction from digital hemispherical photography in boreal forests." *Agricultural and Forest Meteorology*, Vol. 129: pp. 187–207. doi: 10.1016/j.agrformet.2004.09.006

Maas, H.-G., Bienert, A., Scheller, S., and Keane, E. 2008. "Automatic forest inventory parameter determination from terrestrial laser scanner data." *International Journal of Remote Sensing*, Vol. 29: pp. 1579–1593. doi: 10.1080/01431160701736406

Mariscal, M.J., Martens, S.N., Ustin, S.L., Chen, J., Weiss, S.B., and Roberts, D.A. 2004. "Light-transmission profiles in an old-growth forest canopy: Simulations of photosynthetically active radiation by using spatially explicit radiative transfer models." *Ecosystems*, Vol. 7: pp. 454–467. doi: 10.1007/s10021-004-0137-4

Massaro, R.D., Anderson, J.E., Nelson, J.D., and Edwards, J.D. 2014. "A comparative study between frequency-modulated continuous wave LADAR and linear mode LiDAR." *ISPRS—International Archives of the Photogrammetry, Remote Sensing and Spatial Information Sciences*, Vol. XL-1: pp. 233–239. doi: 10.5194/isprsarchives-XL-1-233-2014.

Medlyn, B., Barrett, D., Landsberg, J., Sands, P., and Clement, R. 2003. "Conversion of canopy intercepted radiation to photosynthate: Review of modelling approaches for regional scales." *Functional Plant Biology*, Vol. 30: pp.153–169.

Mercado, L.M., Huntingford, C., Gash, J.H.C., Cox, P.M., and Jogireddy, V. 2007. "Improving the representation of radiation interception and photosynthesis for climate model applications." *Tellus B*, Vol. 59: pp. 553–565. doi: 10.1111/j.1600-0889.2007.00256.x

Moorthy, I., Miller, J.R., Hu, B., Chen, J., and Li, Q. 2008. "Retrieving crown leaf area index from an individual tree using ground-based lidar data." *Canadian Journal of Remote Sensing*, Vol. 34: pp. 320–332.

Moskal, L.M., and Zheng, G. 2012. "Retrieving forest inventory variables with terrestrial laser scanning (TLS) in urban heterogeneous forest." *Remote Sensing*, Vol. 4: pp. 1–20. doi: 10.3390/rs4010001

Newnham, G., Armston, J., Muir, J., Goodwin, N., Tindall, D., Culvenor, D., Püschel, P., Nyström, M., and Johansen, K. 2012. *Evaluation of Terrestrial Laser Scanners for Measuring Vegetation Structure: A Comparison of the FARO Focus 3D 120, Leica C10, Leica HDS7000 and Riegl VZ1000*. Canberra, Australia: CSIRO.

Nilson, T. 1971. "A theoretical analysis of the frequencey of gaps in plant stands." *Agricultural Meteorlogy*, Vol. 8: pp. 25–38. doi: 10.1016/0002-1571(71)90092-6

Parker, G.G. 1995. "Structure and microclimate of forest canopies." In *Forest Canopies*, edited by M.D. Lowman and N.M. Nadkarni, pp. 73–106. San Diego, CA: Academic Press.

Persistence of Vision Pty. Ltd. 2004. "Persistence of Vision Raytracer (Version 3.6)" [Computer software]. http://www.povray.org/download/. Accessed July 1, 2016.

Pfeifer, N., Gorte, B., and Winterhalder, D. 2004. "Automatic reconstruction of single trees from terrestrial laser scanner data." *ISPRS—International Archives of the Photogrammetry, Remote Sensing and Spatial Information Sciences*, Vol. 35(No. B5): pp. 114–119.

Pharr, M., and Humphreys, G. 2004. *Physically Based Rendering: From Theory to Implementation*. San Francisco, CA: Morgan Kaufmann Publishers.

Piñeiro, G., Perelman, S., Guerschman, J.P., and Paruelo, J.M. 2008. "How to evaluate models: Observed vs. predicted or predicted vs. observed?" *Ecological Modelling*, Vol. 216: pp. 316–322. doi: 10.1016/j.ecolmodel.2008.05.006

Pueschel, P., Newnham, G., and Hill, J. 2014. "Retrieval of gap fraction and effective plant area index from phase-shift terrestrial laser scans." *Remote Sensing*, Vol. 6: pp. 2601–2627. doi: 10.3390/rs6032601

Ramirez, F.A., Armitage, R.P., and Danson, F.M. 2013. "Testing the application of terrestrial laser scanning to measure forest canopy gap fraction." *Remote Sensing*, Vol. 5: pp. 3037–3056. doi: 10.3390/rs5063037

Raumonen, P., Kaasalainen, M., Åkerblom, M., Kaasalainen, S., Kaartinen, H., Vastaranta, M., Holopainen, M., Disney, M., and Lewis, P. 2013. "Fast automatic precision tree models from terrestrial laser scanner data." *Remote Sensing*, Vol. 5: pp. 491–520. doi: 10.3390/rs5020491

Seidel, D., Fleck, S., and Leuschner, C. 2012. "Analyzing forest canopies with ground-based laser scanning: A comparison with hemispherical photography." *Agricultural and Forest Meteorology*, Vol. 154–155: pp. 1–8. doi: 10.1016/j.agrformet.2011.10.006

Strahler, A.H., Jupp, D.L., Woodcock, C.E., Schaaf, C.B., Yao, T., Zhao, F., Yang, X., et al. 2008. "Retrieval of forest structural parameters using a ground-based lidar instrument (Echidna®)." *Canadian Journal of Remote Sensing*, Vol. 34: pp. S426–S440. doi: 10.5589/m08-046

Stuckens, J., Somers, B., Delalieux, S., Verstraeten, W., and Coppin, P. 2009a. "The impact of common assumptions on canopy radiative transfer simulations: A case study in citrus orchards." *Journal of Quantitative Spectroscopy and Radiative Transfer*, Vol. 110: pp. 1–21. doi: 10.1016/j.jqsrt.2008.09.001

Stuckens, J., Verstraeten, W.W., Delalieux, S., Swennen, R., and Coppin, P. 2009b. "A dorsiventral leaf radiative transfer model: Development, validation and improved model inversion techniques." *Remote Sensing of Environment*, Vol. 113: pp. 2560–2573. doi: 10.1016/j.rse.2009.07.014

Szeliski, R. 1993. "Rapid octree construction from image sequences." *CVGIP: Image Understanding*, Vol. 58: pp. 23–32.

Vaccari, S., Van Leeuwen, M., Calders, K., Coops, C., and Herold, M. 2013. "Bias in lidar-based canopy gap fraction estimates." *Remote Sensing Letters*, Vol. 4: pp. 391–399.

Van der Zande, D., Hoet, W., Jonckheere, I., van Aardt, J., and Coppin, P. 2006. "Influence of measurement set-up of ground-based LiDAR for derivation of tree structure." *Agricultural and Forest Meteorology*, Vol. 141: pp. 147–160. doi: 10.1016/j.agrformet.2006.09.007

Van der Zande, D., Jonckheere, I., Stuckens, J., Verstraeten, W.W., and Coppin, P. 2008. "Sampling design of ground-based lidar measurements of forest canopy structure and its effect on shadowing." *Canadian Journal of Remote Sensing*, Vol. 34: pp. 526–538. doi: 10.5589/m08-070

Van der Zande, D., Stuckens, J., Verstraeten, W., Muys, B., and Coppin, P. 2010. "Assessment of light environment variability in broadleaved forest canopies using terrestrial laser scanning." *Remote Sensing*, Vol. 2: pp. 1564–1574. doi: 10.3390/rs2061564

Van der Zande, D., Stuckens, J., Verstraeten, W.W., Mereu, S., Muys, B., and Coppin, P. 2011. "3D modeling of light interception in heterogeneous forest canopies using ground-based LiDAR data." *International Journal of Applied Earth Observation and Geoinformation*, Vol. 13: pp. 792–800. doi: 10.1016/j.jag.2011.05.005

Van Leeuwen, M., Coops, N., Hilker, T., Wulder, M., Newnham, G., and Culvenor, D. 2013. "Automated reconstruction of tree and canopy structure for modeling the internal canopy radiation regime." *Remote Sensing of Environment*, Vol. 136: pp. 286–300. doi: 10.1016/j.rse.2013.04.019

Van Leeuwen, M., Hilker, T., Coops, N.C., Frazer, G., Wulder, M.A., Newnham, G.J., and Culvenor, D.S. 2011. "Assessment of standing wood and fiber quality using ground and airborne laser scanning: A review." *Forest Ecology and Management*, Vol. 261: pp. 1467–1478. doi: 10.1016/j.foreco.2011.01.032

Van Leeuwen, M., and Nieuwenhuis, M. 2010. "Retrieval of forest structural parameters using LiDAR remote sensing." *European Journal of Forest Research*, Vol. 129: pp. 749–770. doi: 10.1007/s10342-010-0381-4

Waide, R.B., Willig, M.R., Steiner, C.F., Mittelbach, G., Gough, L., Dodson, S.I., Juday, G.P., and Parmenter, R. 1999. "The relationship between productivity and species richness." *Annual Review of Ecology and Systematics*, Vol. 30: pp. 257–300.

Walter, J.-M.N., Fournier, R.A., Soudani, K., and Meyer, E. 2003. "Integrating clumping effects in forest canopy structure: an assessment through hemispherical photographs." *Canadian Journal of Remote Sensing*, Vol. 29: pp. 388–410.

Wang, M., and Tseng, Y.-H. 2004. "LiDAR data segmentation and classification based on octree structure." *ISPRS—International Archives of the Photogrammetry, Remote Sensing and Spatial Information Sciences*, Vol. 35(No. B3): pp. 308–313.

Wang, M., and Tseng, Y.-H. 2011. "Incremental segmentation of lidar point clouds with an octree-structured voxel space." *The Photogrammetric Record*, Vol. 26: pp. 32–57. doi: 10.1111/j.1477-9730.2011.00624.x

Weiss, M., Baret, F., Smith, G.J., Jonckheere, I., and Coppin, P. 2004. "Review of methods for in situ leaf area index (LAI) determination. Part II. Estimation of LAI, errors and sampling." *Agricultural and Forest Meteorology*, Vol. 121: pp. 37–53. doi: 10.1016/j.agrformet.2003.08.001

Whittaker, E.T., and Robinson, D. 1924. *The Calculus of Observations: A Treatise on Numerical Mathematics* (First ed.). London, UK: Blackie and Son Limited.

Yang, X., Strahler, A.H., Schaaf, C.B., Jupp, D.L.B., Yao, T., Zhao, F., Wang, Z., et al. 2013. "Three-dimensional forest reconstruction and structural parameter retrievals using a terrestrial full-waveform lidar instrument (Echidna®)." *Remote Sensing of Environment*, Vol. 135: pp. 36–51. doi: 10.1016/j.rse.2013.03.020

Zhang, J.X., and Lin, X.G. 2012. "Object-based classification of urban airborne LiDAR point clouds with multiple echoes using SVM." Paper presented at XXII ISPRS Congress, Melbourne, Australia, August 25–September 1.

Zhao, F., Strahler, A.H., Schaaf, C.L., Yao, T., Yang, X., Wang, Z., Schull, M.A., et al. 2012. "Measuring gap fraction, element clumping index and LAI in Sierra Forest stands using a full-waveform ground-based lidar." *Remote Sensing of Environment*, Vol. 125: pp. 73–79. doi: 10.1016/j.rse.2012.07.007